Journal of Drug Delivery Science and Technology 111 (2025) 107138

Contents lists available at ScienceDirect

Journal of Drug Delivery Science and Technology

journal homepage: www.elsevier.com/locate/jddst

Surface area enhanced synthesis of Cu and Ni-based metal-organic frameworks for photocatalytic degradation of malachite green dye and anticancer drug delivery applications

A.H. Hatin Betseba, Y. Christabel Shaji *

Department of Chemistry, Holy Cross College (Autonomous), Nagercoil, Tamil Nadu, India[1]

ARTICLE INFO

Keywords:
Metal-organic frameworks (MOFs)
Photocatalytic degradation
Catalytic activity
Heterogeneous photocatalysis
Drug delivery

ABSTRACT

Metal-organic frameworks (MOFs) have gained attention as fascinating porous materials with a wide range of possible applications. In this study, M-MOFs (M = Cu, and Ni) are synthesized at room temperature by the hydrothermal technique and characterized by XRD, SEM with EDX, TEM with SAED and BET techniques. From XRD analysis, the crystallite size of Cu and Ni-based MOFs was 55.79 and 62.2 nm. Moreover, Cu-based MOF exhibited cubic-shaped morphology and Ni-based MOF exhibited leaf-life morphology. The synthesized M-MOFs were demonstrated for photocatalytic performance in the degradation of malachite green dye under UV–visible light irradiation and the cisplatin encapsulated Cu and Ni-based MOF is tested against MDA-MB-231 cell line by MTT assay. Remarkably, Cu-based MOF demonstrated exceptional catalytic activity with a degradation percentage of 97.61 % after 130 min, outperforming Ni-based MOF with a degradation percentage of 84.76 % after 130 min in the breakdown of malachite green dye. The optimal state for Cu-MOF-mediated degradation is identified, showcasing its efficiency in breaking down the dye molecules. Cis@Cu-based and Cis@Ni-based MOFs showed a cell viability of 34.64 % and 37.87 % with IC_{50} values of 47.77 μg/ml and 55.31 μg/ml. The findings indicate that the synthesized MOFs show significant promise in heterogeneous photocatalysis for environmental treatment and anticancer drug delivery.

1. Introduction

Nanotechnology is one of the most active subfields of material science research which finds application in different applications. Nanomaterials are materials with characteristic dimensions on the nanometre scale, typically ranging from 1 to 100 nm. At this scale, materials often exhibit unique properties that differ from their bulk counterparts due to quantum mechanical effects and increased surface area to volume ratio [1]. One area of study in material science is the Metal-Organic Framework (MOF), a type of crystalline material with a distinctive structure made up of metal nodes or clusters connected by organic ligands. An organic linker and metal ions or clusters combine to form a three-dimensional structure with precisely defined and adjustable nanopores [2]. Because of their remarkable surface area and high porosity, MOFs are noteworthy for a variety of applications like batteries [3], supercapacitors [4], gas storage and separation [5], biomedicine [6], chemical sensors [7], proton conductivity [8] and heterogeneous catalysis [9]. Among these, the MOFs have demonstrated significant potential in the realm of photocatalysis, particularly in the breakdown of organic dyes [10].

The environment has been exposed to several undesirable, hazardous compounds due to the rapid rise in industrialization and population. A plethora of synthetic dyes, estimated to be over 700000 tons overall, are released untreated into aquatic environments because of their intrinsic qualities, which include deep chromaticity, resistance to oxidative degradation and chemical and photolytic stability [11]. The water contamination is caused mainly due to the discharge of wastewater from the paper, textile, tannery and pharmaceutical industries. However, the primary cause of pollution in the environment is the textile sector [12]. Due to the presence of organic and inorganic pollutants, dye effluent is extremely carcinogenic and mutagenic in nature and lacks biodegradability. If it is not properly handled, it can be released into natural ecosystems, which poses a major risk to human health and the environment [13]. Among these, Malachite green (MG) is a water-soluble

* Corresponding author.
E-mail addresses: christabelshaji@holycrossngl.edu.in, shajichristabel@gmail.com (Y.C. Shaji).
[1] Affiliated to Manonmaniam Sundaranar University, Tirunelveli

https://doi.org/10.1016/j.jddst.2025.107138
Received 18 June 2024; Received in revised form 21 May 2025; Accepted 2 June 2025
Available online 3 June 2025

basic dye, classified as a diamino derivative within the triphenylmethane class of dyes. It is widely utilized in the aquaculture sector due to its high effectiveness against fungal and protozoan infections. On the other hand, it is also utilized as a food colouring agent, food additive, medical disinfectant as well as a dye in acrylic industries, paper, jute, wool, silk, cotton and leather [14]. However, due to its potential toxicity towards aquatic organisms and environmental persistence, its use in certain applications has been restricted or banned in many countries. Exposure time, temperature and concentration all increase the dye's toxicity. Organ damage, mutagenic, carcinogenic and developmental abnormalities are all symptoms of toxicity in some mammals [15]. Carcinogenesis, mutagenesis, chromosomal fractures, teratogenicity and pulmonary toxicity have all been described as symptoms caused due to toxicity from the consumption of malachite green. Recently, many MOF materials have been successfully employed to decolorize a variety of dyes in aqueous solutions. These materials include MIL-125 [16], MOF-5 [17], MIL-101 [18]. Previous investigations have already shown that metal-organic frameworks, particularly uranyl-based coordination polymers showed encouraging photocatalytic dye pollution degradation in the presence of UV, visible and UV–visible illumination [19]. Also, the semiconductor characteristics of metal-organic frameworks make them highly suitable for the photocatalytic breakdown of organic contaminants [20]. Xing et al. reported that NNU-36 acted as a highly effective heterogeneous photocatalyst for the breakdown of Rhodamine (RhB), Rhodamine 6G (R6G), Methylene blue (MB) dyes and for the reduction of aqueous Cr(VI). Under the influence of visible light, the photocatalytic degradation of RhB, R6G and MB by NNU-6 in the presence of an environmentally safe oxidant H_2O_2 demonstrated a degradation of 96.2 % after 70 min, 93.5 % after 90 min and 94.2 % after 80 min. These and other results underscore the significant potential of MOFs for photocatalytically removing environmental contaminants [21]. However, synthesizing M-MOFs at a large scale with consistent properties such as uniform pore size and crystallinity remained a major drawback. Many MOFs were reported to degrade in water or under acidic or alkaline conditions. For instance, HKUST-1 showed poor hydrolytic stability, leading to reduced efficiency in dye adsorption over time. But Cu and Ni-based MOFs showed no solubility in water and degraded the dye with the greatest efficiency. The cost-effectiveness for dye removal by Cu and Ni-based MOFs was quite affordable than other conventional methods like activated carbon adsorption, chemical coagulation/flocculation, membrane filtration and advanced oxidation processes as it requires high operational costs, high intensive energy for regeneration and sludge production.

Regrettably, cancer ranks among the world's major causes of mortality for millions of individuals. Cancer deaths are still high despite significant advancements in cancer biology during the past ten years. Poor biological distribution, unfavourable side effects and poor pharmacokinetics are some of the drawbacks of traditional cancer treatments [22]. Although chemotherapy is the most widely used cancer treatment, it has a number of disadvantages, the most important of which are adverse effects on normal cells and limited therapeutic efficacy during the course of treatment. Breast cancer is the most common cancer among women diagnosed globally. It can be classified into three main subgroups according to the presence of three important markers: human epidermal growth factor receptor 2 (HER2), estrogen receptor (ER) and progesterone receptor (PR) [23]. Nonetheless, 15–20 % of all occurrences of breast cancer are triple-negative tumours, which do not express ER, PR or HER2. There is a lower chance of recovery for these tumours, which are believed to be the most serious kind of breast cancer [24]. Zeolitic imidazole frameworks (ZIFs) are a particularly promising class of metal-organic frameworks (MOFs) because of their advantageous structures, which include large pore volumes, intrinsic biodegradability and large surface areas with zinc ions and 2-methyl imidazolate. They are also known for their high thermal and hydrothermal stability, non-toxicity and biocompatibility [25]. Consequently, ZIF-8 has been recognized as a viable drug delivery nanocarrier [26] and controlled release of small molecules, including gases, fluorescent probes and therapeutic agents. In 2019, using post-synthetic stirring of dried ZIF-8 powder with Doxorubicin in an aqueous solution, ZIF-8 is effectively loaded by the Junior group with 4.9 wt% of DOX. The drug is released very gradually and under strict control and after 30 days 66 % drug is released [27]. Similarly, ZIF-8 is employed as a pH-responsive drug carrier vehicle for the delivery of 5-fluorouracil (5-FU). By post-synthesis alteration of ZIF-8 with 5-FU, an incredible amount of the drug is established. Studies revealed that the drug is released more quickly in a little acidic buffer solution of pH 5.0 than in a neutral environment of pH 7.4 [28]. The main advantage of Cu and Ni-based MOFs is the loading of the anticancer drug Cisplatin by simple impregnation method and the precise control over drug release at a pH of 7.4. Moreover, the Cisplatin-loaded Cu and Ni-based MOFs cause damage only to the cancerous cell line with low toxicity towards the normal cell line. The cost-effectiveness is quite affordable.

This study's aim and objectives involve synthesizing novel Cu and Ni-based MOFs using copper and nickel as metal precursors, benzene 1,3,5-tricarboxylic acid as ligands and DMSO as solvent by the hydrothermal method in a stainless-steel Teflon autoclave and the loading of the anticancer drug Cisplatin inside Cu and Ni-based MOFs by impregnation method which is never reported before. The as-synthesized MOFs were characterized by XRD, SEM, TEM and N_2 sorption isotherm and examined their activities for the photocatalytic degradation of Congo red dye under UV–visible light irradiation and the Cisplatin incorporated Cu and Ni-based MOFs as a drug carrier against Breast cancer cell line MDA-MB-231 and evaluated their antiproliferative effect by MTT assay.

The structure of the present study is organized as follows, in section 2, the material and methods of the study are given. In section 3, the photocatalytic degradation of malachite green using Cu and Ni-based MOF under UV–visible light irradiation is reported. The Cu-based MOF showed a degradation of 97.61 % after 130 min while the Ni-based MOF showed only 84.76 % after 130 min. To have more understanding of the photocatalytic degradation mechanism of malachite green dye, the properties of the synthesized MOFs has been linked to catalytic efficiency and the proposed mechanism is well discussed. Also, the cytotoxicity of cisplatin-loaded Cu and Ni-based MOFs have been examined against breast cancer cell line MDA-MB-231 by MTT assay is also reported. At higher concentrations of 100 μg/ml, the cell viability of Cu and Ni-based MOFs are found to be 34.64 % and 37.87 % with IC_{50} values of 47.77 μg/ml and 55.31 μg/ml and in section 4, the present study is concluded.

2. Materials and methods

2.1. Chemicals

Copper nitrate hexahydrate, nickel nitrate hexahydrate, 1,3,5 benzene tricarboxylic acid, acetonitrile, dimethyl sulphoxide, Cisplatin, malachite green dye. MDA-MB-231 cell line is purchased from the National Centre for Cell Sciences, Pune. All the chemicals are used without further purification.

2.2. Synthesis

2.2.1. Synthesis of Cu-based MOFs

The Cu-based MOF is prepared by the Teflon Autoclave using the hydrothermal method based on the synthesis process. $Cu(NO_3)_2{\cdot}6H_2O$ (0.1455 mmol) is dissolved in 10 ml deionized water (sol A) and benzene 1,3,5 tricarboxylic acid (0.18 mmol) is dispersed in 20 ml DMSO (sol B). Sol A is slowly added to sol B with continuous stirring and to create a reaction mixture, 10 ml of CH_3CN is added with stirring at room temperature. After that, the mixture is put in a 100 ml Teflon flask and placed in an oven that is heated to 150 °C for 12 h. After cooling, the solution is centrifuged, and the precipitate is collected. The material is

rinsed three more times to get rid of contaminants. Finally, the product is dried at 80 °C for 3 h.

2.2.2. Synthesis of Ni-based MOFs

The Ni-based MOF is prepared using a stainless-steel Teflon autoclave by hydrothermal method, based on the synthesis process. Ni $(NO_3)_2{\cdot}6H_2O$ (0.0145 mmol) is dissolved in 10 ml deionized water (sol A) and benzene 1,3,5 tricarboxylic acid (0.18 mmol) is dispersed in 20 ml DMSO (sol B). Sol A is added to sol B with constant stirring and at room temperature and 10 ml of CH_3CN is added to create a clear solution. The mixture is then put into a 100 ml Teflon flask and put into a reactor that is heated to 150 °C for 12 h. Centrifugation is used to gather the precipitate once it cooled. The material underwent three further washings to eliminate contaminants. The final step is drying the product at 80 °C for 3 h.

2.2.3. Encapsulation of cisplatin

Both the Cu and Ni-based MOFs are used for the encapsulation of Cisplatin. This is accomplished by liquid impregnation method. Before the encapsulation of Cisplatin, both the MOFs are dehydrated at 150 °C to get rid of water molecules from the MOF's pores. About 300 mg of both MOFs are soaked in the cisplatin solution (cis [Pt $(NH_3)_2Cl_2$]). The encapsulation process is carried out for 48 h with constant stirring a normal atmosphere, then the resulting product is centrifuged, and the samples are left to air dry. The Cisplatin loaded Cu and Ni-based MOFs have been evaluated on breast cancer MDA-MB-231 cell lines.

2.2.4. Methodology for drug loading estimation

The amount of cisplatin loaded into the MOFs is estimated using UV–Vis spectrophotometry. Briefly, the supernatant from the cisplatin loading step is collected after centrifugation, and the concentration of unencapsulated drug is measured using a UV–Vis spectrophotometer. Drug loading efficiency and encapsulation efficiency were then calculated using the difference between the initial and residual drug concentrations.

$$\text{Drug loading capacity} = \frac{(\textit{weight of MOF}) - (\textit{weight of drug loaded MOF})}{\textit{Weight of MOF}} X100$$

2.3. Characterization

For the characterization of copper and nickel-based MOFs different methods are used. Using a Bruker binary V4 X-ray diffractometer with Cu Kα (1.5406 Å) irradiation in the range of 0–80°, XRD analysis is used to examine the phase purity and crystal structure of samples. The Quanta FEG-250 SEM is utilized to examine the structure of the particles in the samples, while energy-dispersive X-ray microanalysis (EDS) is employed to analyze the composition. and transmission electron microscopy (TEM) using the JEOL-2100+ instrument working at 200Kv. The BET surface area for the synthesized samples is examined by N_2 sorption isotherm at 77 K using Quantachrome Nova 1200. The sample is degassed before the analysis for 3.3 h with the final outgas temperature maintained at 120 °C.

2.4. Photocatalytic degradation of malachite green dye

The malachite green dye is then broken down by the MOF acting as a photocatalyst. The electrons in the MOF are excited by a light source, usually UV visible light, creating electron-hole pairs that result in dye degradation.

Approximately 0.001 g (1 ppm) of malachite green dye is dissolved in 1000 ml of double-distilled water to create a solution for photocatalytic study. To 40 ml of dye solution, approximately 0.05 g of the catalyst is added and the mixture is stirred thoroughly in the dark to ensure an even distribution of the dye in the photocatalyst suspension. The beaker containing the photocatalyst solution is then positioned under a light source to achieve uniform irradiation of the solution. The experiment is initiated, and the start time (t = 0) is recorded. Samples are collected at regular time intervals (0, 15, 25, 35, 50, 65, 80 and 130 min), each consisting of approximately 4 ml from the reaction mixture. These samples are subsequently analyzed using UV–Vis spectroscopy.

2.5. Cell culture and maintenance

The cells are grown in Dulbecco's Modified Eagle's Medium (DMEM-Himedia). It is supplemented with 1 % antibiotic cocktail (consisting of Amphotericin B (2.5 μg/ml), Streptomycin (100 μg/ml), and Penicillin (100 U/ml) and 10 % heat-inactivated fetal bovine serum (FBS). A cell culture incubator (Galaxy® 170, Eppendorf, Germany) with 5 % CO_2 at 37 °C and humidity is used to cultivate the cells in TC flasks (25 cm^2).

2.5.1. Cytotoxicity test by MTT assay

After being planted on 96-well plates, the cells (2500 cells/well) are given a full day to adjust to the culture conditions in the incubator, which included 37 °C and 5 % CO_2. The DMEM media (10 mg/ml) is used to prepare the test samples, which are then filtered and sterilized with a Millipore syringe filter of 0.2 μm. After further dilution with DMEM fluid, the samples are added at final concentrations of 6.25, 12.5, 25, 50 and 100 μg mL^{-1}, respectively, to the wells holding cultivated cells. As a control, untreated wells are maintained. To reduce errors, every test is performed three times and average values are recorded. Following the application of test samples, the plates underwent a period of incubation of 24 h. The media from the wells are aspirated and disposed of following the incubation period. The wells are filled with 0.5 mg/ml MTT solution of 100 μL in phosphate buffer solution. In order to encourage the formation of formazan crystals, the plates underwent an additional 2 h of incubation. After removing the supernatant, each well is added with 100 μL of 100 % DMSO.

3. Results and discussion

In this section, the outcome of the characterization method of nickel and copper metal-organic framework (MOFs) is analyzed.

3.1. XRD analysis

X-ray diffraction technique is performed to identify the phase formation and crystallographic information of the samples. The XRD analysis of Cu and Ni-based MOFs are carried out by Bruker binary V4 X-ray diffractometer with Cu Kα radiation (1.5406 Å) and scanning over the 2θ range from 10 to 80°. XRD patterns of Cu and Ni-based MOFs by hydrothermal method and drying at 80 °C for 3 h are displayed in Fig. 1. The patterns exhibited narrow diffraction peaks which indicated well defined crystalline nature of the sample.

From Fig. 1(b), the peaks in the XRD spectra indicated distinctive features for Cu-MOFs, with high-intensity diffraction peaks observed at 2θ = 17.28, 24.8, 27.92 and 29.16 corresponding to the planes of (1 1 1), (2 0 0), (2 1 1) and (2 2 0) as well as lower intensity peaks at 2θ = 12.2, 35.08 corresponding to the planes of (1 1 0) and (3 1 0). The most prominent peak for Cu-MOFs appeared at 2θ = 17.37. The crystallographic patterns of Cu-MOFs revealed a simple cubic crystal structure, evidenced by well-defined, sharp peaks, highlighting its highly crystalline nature [29]. From Fig. 1(a), Ni-based MOFs showed peaks at 2θ = 12.56, 15.4, 17.32, 19.92, 20.4, 24.04, 25.24, 27.88, 29.6, 31.76, 32.64, 37.28, 38.24, 39.56, 40.96, 50.12. The most intense peaks at 27.88 and 29.6 correspond to the plane (1 1 1) and (2 0 0) [30]. The Scherrer equation is utilized to determine the mean crystalline dimensions,

$$D = \frac{K\lambda}{\beta \text{Cos}\theta}$$

Where D is the average crystallite size (nm), λ is the X-ray wavelength of

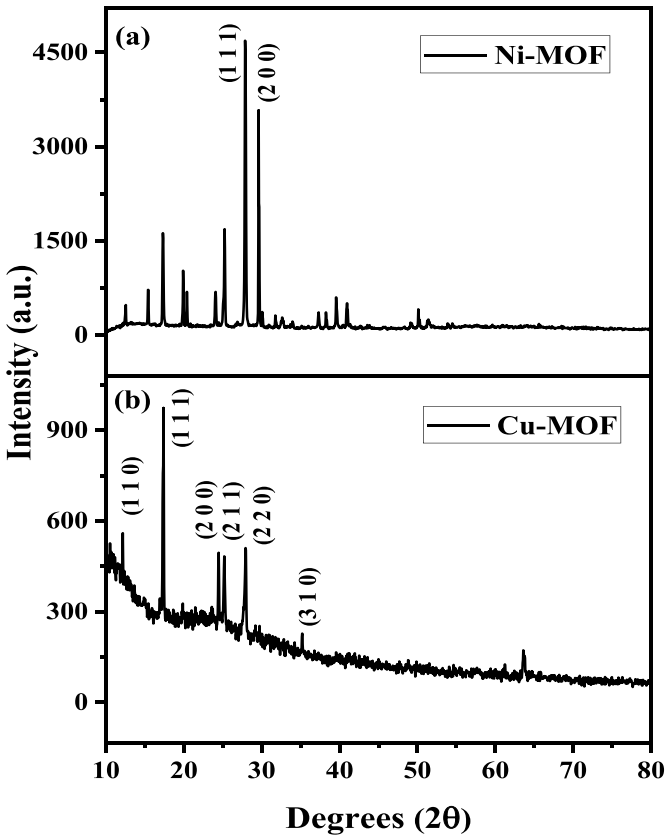

Fig. 1. Xrd of Cu and Ni-based MOFs.

CuKα (0.154 nm), β is the full-width half maximum (FWHM) of the most intense diffraction peaks and θ is the Bragg angle. The determined average size of Cu and Ni-based MOFs is found to be 55.79 and 62.2 nm, respectively.

3.2. SEM with EDX analysis

Scanning electron microscopy (SEM) and Energy dispersive x-ray spectroscopy (EDX) analyses are used to examine the surface morphology, aggregation and composition of the prepared Cu and Ni-based MOFs. The SEM images of the Cu and Ni-based MOFs formed are shown in Fig. 2. The focus images on the Cu-based MOFs revealed their formation as distinct and well-defined uniform cubic clusters of fine shapes either as separated or aggregated forms (Fig. 2(a&b)). The cubic shapes of Cu-based MOF are of size range from 20 to 60 μm. Additionally, EDX analysis is utilized for chemical characterization and elemental analysis of the catalyst (Fig. 2 (c)). The different energy peaks correspond to the different elements in the sample. The elements carbon, oxygen, sulphur and copper are confirmed to be present in the sample by the analysis [31]. The focus image on the Ni-based MOFs exhibited their formation as a leaf-like morphology that interlaced with each other and formed a structure resembling a nest. The leaf-shaped Ni-based MOF are of lateral size range 40–70 μm (Fig. 2(d&e)) [32]. EDX analysis confirmed the presence of carbon, oxygen, sulphur and nickel which relate to the organic ligands and metal in the final structure of Ni-based MOF (Fig. 2 (f)). Such morphological properties play a vital role in enhancing the photocatalytic activity of Cu and Ni-based MOFs by interacting with the incident light photons during the photocatalytic degradation of malachite green dye.

3.3. TEM with SAED analysis

TEM analysis is further used to demonstrate the more detailed morphology of Cu and Ni-based MOFs. Fig. 3(a&b), depicts the uniform cubic clusters morphology of Cu-based MOFs and indicates that the Cu nanoparticles are well dispersed on the MOFs. The formation is further confirmed from the lattice spacing observed from the TEM image of Cu-based MOFs. The d-spacing of the Cu crystal is determined as 0.23 nm, corresponding to the (1 1 1) crystallographic plane of Cubic Cu [33]. From Fig. 3(d&e) the TEM image makes it evident that Ni-based MOF comprises several nanosheets and a uniform cavity with a comparatively smooth surface. The d-spacing of the Ni crystal is determined as 0.32 nm, corresponding to the (1 1 1) crystallographic plane [34]. The SAED pattern of Cu-based MOF and Ni-based MOF shown in Fig. 3(c&f), depict the clear diffraction sports confirming the crystalline structure of samples.

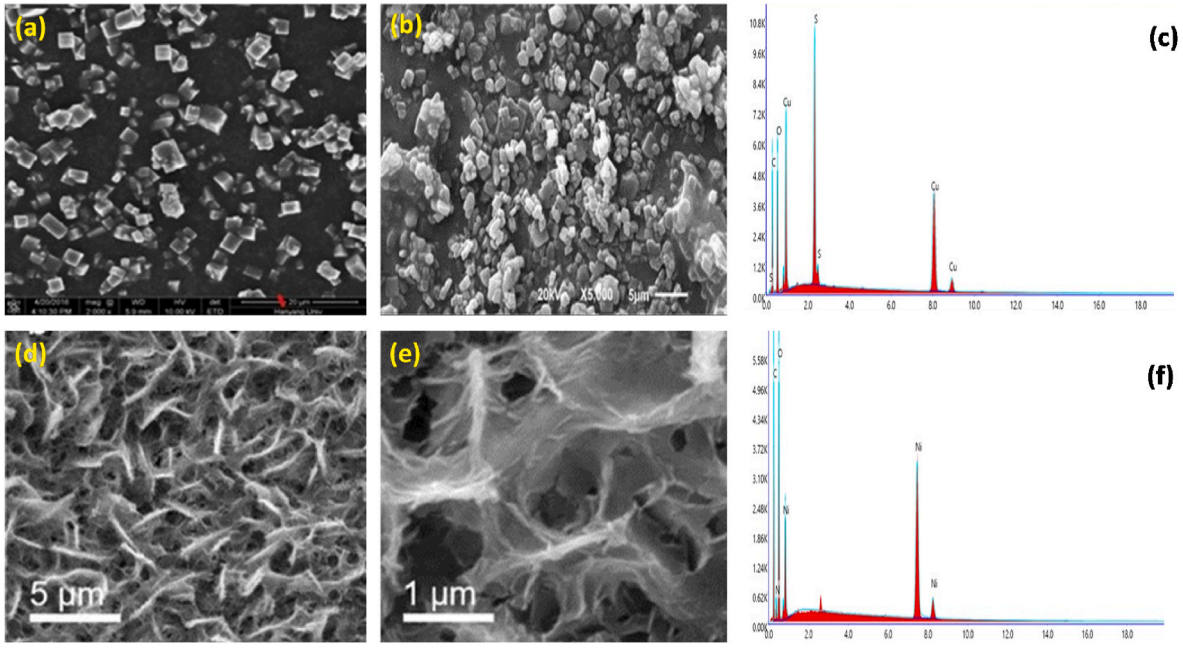

Fig. 2. (a&b) SEM images of Cu-based MOF, (c) EDX of Cu-based MOF, (d&e) SEM images of Ni-based MOF and (f) EDX of Ni-based MOF.

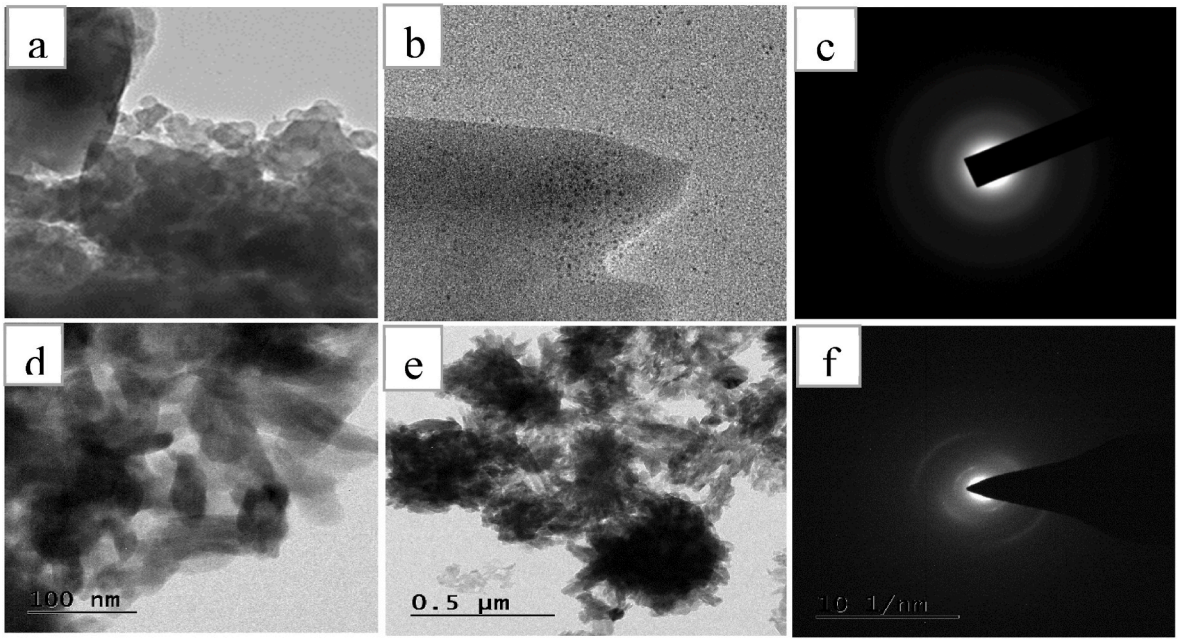

Fig. 3. TEM with SAED images of Cu-based MOF (a, b, c), Ni-based MOF (d, e, f).

3.4. UV–Vis spectroscopy analysis

To evaluate the optical properties and confirm the successful incorporation of cisplatin into the MOFs, UV–Vis absorption spectroscopy is performed on both MOFs and cisplatin-loaded MOFs. As shown in Fig. 4 (a), the Cu-based MOF exhibits a characteristic broad absorption band in the UV–Vis region, which significantly intensifies upon loading with cisplatin (Cis@Cu-based MOF). A similar trend is observed in the Ni-based system (Fig. 4(b)), where Cis@Ni-based MOF displays markedly higher absorbance compared to the bare Ni-based MOF. The enhanced absorption is attributed to the presence of cisplatin molecules within the porous MOF structure, as well as potential interactions between the drug and the metal nodes. The optical band gaps were estimated using Tauc plot analysis derived from UV–Vis absorption spectra. Assuming an indirect allowed transition, the Tauc relation $(\alpha h\nu)^{1/2} = A\,(h\nu - Eg)$ was applied, where α is the absorption coefficient, hν is the photon energy, A is a constant, and Eg is the optical band gap. The extrapolation of the linear region of the $(\alpha h\nu)^{1/2}$ versus hν plot allowed the determination of the optical band gap energies. The bandgaps of Cu and Ni-based MOFs are found to be 2.15 and 2.27 eV [35,36]. These results not only confirm the successful integration of cisplatin but also highlight the potential of Cu and Ni based MOFs as photoactive materials for biomedical and photocatalytic applications (see Fig. 5).

3.5. BET surface analysis

The Brunauer-Emmett-Teller (BET) and Barrett-Joyner-Halenda (BJH) characterization techniques are applied to evaluate and understand the effect on the specific surface area, pore volume, pore diameters and kind of isotherms of the Cu and Ni-based MOFs. For all materials, the nitrogen sorption measurements are carried out at 77 k. It is based on the adsorption of gas molecules onto the surface of the material. The principle involves the use of the BET equation, which relates the amount of gas adsorbed at a given pressure to the surface area of the material. By measuring the amount of gas adsorbed at different pressures, the BET method can calculate the surface area of the material. The shape of isotherm of both Cu and Ni-based MOFs according to Brunauer-Emmett-Teller classification is nearly of type IV isotherm thus indicating a mesoporous nature of samples. The surface area is not an important factor in the enhanced photocatalytic activity of Cu and Ni-based MOFs. The main factor responsible for the superior photocatalytic activity of Cu and Ni-based MOFs could be attributed to extended light absorption and

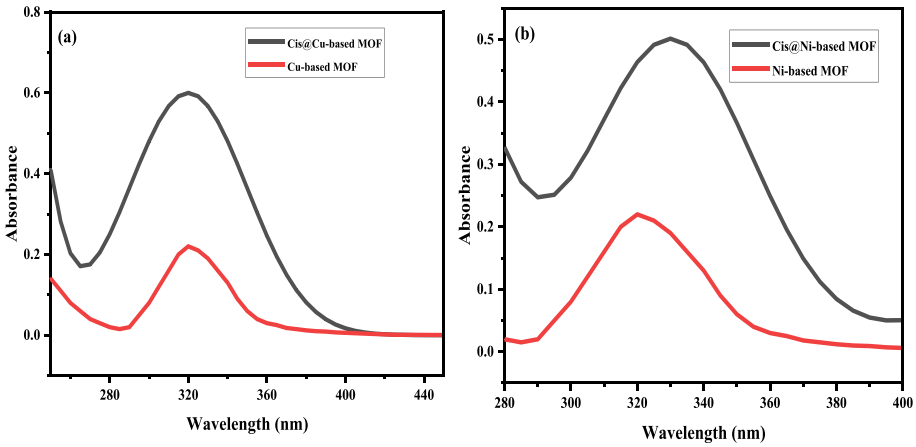

Fig. 4. UV–Vis spectroscopy of (a) Cu-based MOF (b) Ni-based MOF.

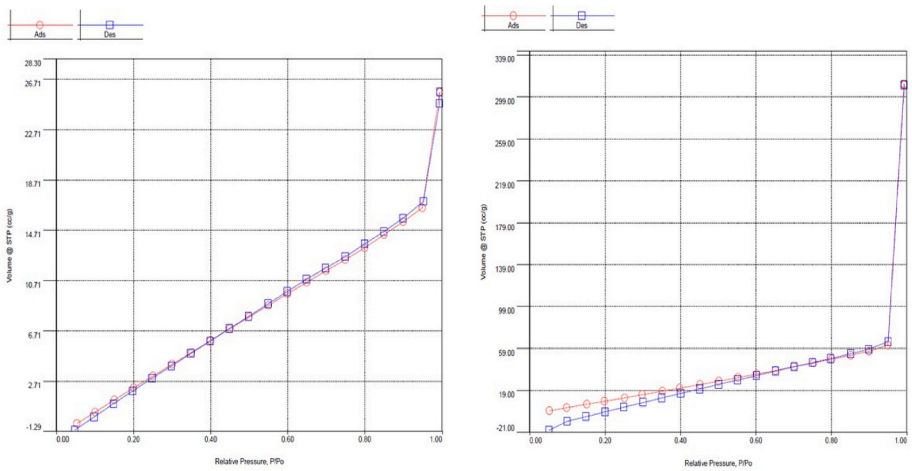

Fig. 5. N_2 sorption isotherms of Cu and Ni-based MOFs.

improved electron-hole separation of Cu and Ni-based MOFs. The BET surface area is displayed in Table 1.

Based on the calculations of nitrogen adsorption-desorption, the Cu-MOF has a higher value than the Ni-MOF. Cu-MOF obtained the highest surface area (594 m^2/g) and pore volume (0.532 cm^3/g). Thus, the analysis proves Cu is better the Ni particles [37,38].

3.6. Photocatalytic activity

The UV–Vis spectra of malachite green dye exhibited a peak at 598 nm in the absence of a Cu-based MOF catalyst. For MOFs to catalyze the photocatalytic degradation of dyes, metal centers must be present. These metal centers unique characteristics provide active locations for interactions with dye molecules, enhance charge transfer and allow the start of redox processes. In the absence of the catalyst, the prerequisites for effective photocatalysis might not be satisfied which suggests that malachite green dye is stable and doesn't undergo degradation without catalysts under UV–visible light. Upon the addition of 0.05 g of the Cu-based MOF catalyst, a reduction in the λ_{max} value of the spectra corresponding to the peak at 598 nm, with no emergence of additional peaks at different time intervals is observed. The peaks associated with malachite green dye exhibited a continuous decrease, indicative of the progressive dye degradation. In the presence of UV–Vis light, the malachite green dye is degraded for up to 130 min.

The superior performance of Cu-based MOF is attributed to its unique catalytic properties, such as better absorption of light and superior separation of charge capabilities. The photocatalytic activity of Cu-based MOF has demonstrated its potential as an effective and sustainable solution for removing malachite green dye from aqueous solutions.(see Fig. 6)

Using the following formula, the percentage of malachite green deterioration is determined:

$$\% \text{ of degradation} = A_0 - A_t \,/\, A_0 \text{ x } 100$$

Where A_0 signifies the absorbance at time t = 0 and A_t signifies the absorbance after time t of treatment. A_0 and A_t are recorded at λ_{max} of dye.

From the analysis, the Cu-based MOFs have a higher degradation percentage of about 97.61 % after 130 min. In contrast, the degradation percentage of Ni-based MOFs is only 84.76 % after 130 min, which made Cu-based MOFs superior to Ni-based MOFs. The superior performance of Cu-based MOF is attributed to metal selection, band structure, MOF pore size, light absorption and excitation, charge transfer and separation properties. The surface of MOFs with active sites can vary in their affinity for malachite green dye molecules and their ability to promote photocatalytic reactions. The coordination chemistry of copper and nickel ions within the MOF resulted in different reactivity toward the dye molecules. Compared to Ni-based MOF, the Cu-based is found to have large pore size and surface area which leads to better adsorption of malachite green dye and improved degradation rates. Copper-based MOFs exhibited better light absorption properties in the visible range, making them more effective for photocatalysis. This enhanced light absorption can lead to the generation of more pairs of electrons and

Table 2
Photocatalytic performance of other MOFs for the degradation of dyes.

Catalyst	Dye	Source	Time	Degradation %
MIL-53(Fe)	Methylene blue	UV light UV light, H_2O_2	1hr 30 min	17 % [41] 99 %
MOF-199	BB41	UV light	3 h	99 % [42]
Fe_3O_4@MIL-100 (Fe)	Methylene blue	UV light, H_2O_2	1hr	99 % [43]

Table 3
MTT assay of Cis@Cu-based and Cis@Ni-based MOFs.

	Cis@Cu-based MOF		Cis@Ni-based MOF	
Concentrations (μg/ml)	% of viability	% of growth inhibition	% of viability	% of growth inhibition
6.5	94.32	5.68	94.47	5.53
12.5	79.70	20.3	82.47	17.53
25	58.72	41.28	59.56	40.44
50	46.82	53.18	50.01	50.01
100	34.64	65.36	37.87	62.13

Table 1
Surface area analysis.

MOFs	BET surface area (m^2/g)	Micropore volume (cm^3/g)	Average pore diameter (nm)	Crystallite size (nm)
Cu-MOFs	594	0.532	1.721	55.79
Ni-MOFs	521	0.478	1.523	62.2

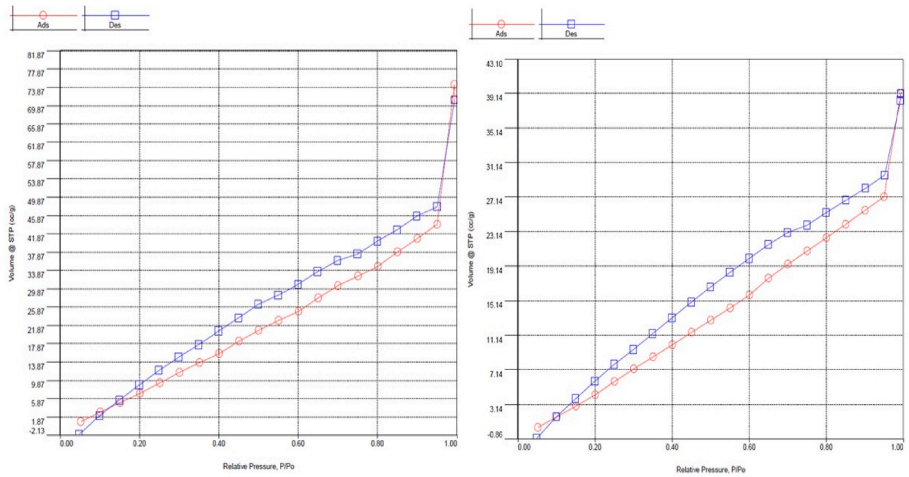

Fig. 6. N_2 sorption isotherms of Cis@Cu-MOF and Cis@Ni-MOF

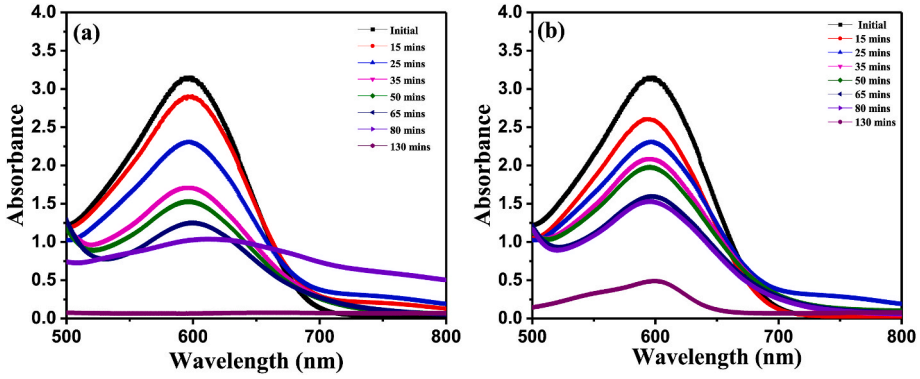

Fig: 7. (a)&(b)UV–Vis spectrum of Malachite green dye using Cu and Ni-based MOFs as a catalyst. (For interpretation of the references to colour in this figure legend, the reader is referred to the Web version of this article.)

holes, which can then participate in the breakdown of malachite green dye. The efficiency of charge separation and transfer processes in the MOF is crucial for photocatalysis. Copper-based MOFs exhibited superior charge separation and transfer properties, allowing for faster and more effective degradation of the dye than Ni-based MOFs. The photocatalytic activity of Cu-based MOFs has demonstrated its potential as an effective and sustainable solution for removing malachite green dye from aqueous solutions.(see Fig. 7)

Nayak et al. reported the efficiency of eliminating the malachite green dye using two different additions as photocatalysts: ZnO and ZnO-TiO_2 nanoparticles. Microwave-assisted combustion and co-precipitation methods have been used to produce nanosized ZnO-TiO_2 and ZnO, respectively. The dye solution containing every metal oxide is exposed to UV and solar radiation and it is observed until it completely lost its colour. The findings showed that, when exposed to sunlight, ZnO-TiO_2 nanoparticles perform the best photocatalytically when compared to ZnO and TiO_2 nanoparticles. The effects of pH change and dose are also investigated. Under sunlight, the dye degraded with the highest efficiency of 92 % at pH 5.8 [39]. Yao et al. synthesized a composite of titanium dioxide and covalent organic framework (TiO_2/COF) and investigated its photocatalytic dye removal properties. The sol-gel process is utilized to manufacture TiO_2 nanomaterial, with tetrabutyl titanate serving as the titanium source. By employing melamine and 1, 4-phthalaldehyde as ligands in solvothermal synthesis, a TiO_2/COF core-shell composite was created in the presence of TiO_2. Using malachite green as a model dye effluent, the photocatalytic decomposition rate of TiO_2/COF composites under UV light irradiation is investigated. The findings demonstrated that altering COF considerably raises TiO_2's photocatalytic efficiency. The degradation rate rises from 69.77 % to 93.64 %. The mechanism of degradation of TiO_2/COF as a photocatalyst is explored and the viability of malachite green breakdown is examined, all based on the free radical capture experiment [40].(See Table 2)

3.6.1. *Photocatalytic degradation mechanism*

The semiconductor theory could be used to analyze the reaction mechanism for the photocatalytic degradation of malachite green dye. According to earlier research, the process known as ligand-to-metal charge transfer (LMCT) involves the movement of electrons from the photoexcited organic ligand to the metal within MOFs, facilitating the photocatalytic degradation of dyes [44].

Due to the presence of metal ions and organic ligands, MOFs used as catalysts can absorb UV–visible light. The formation of the MOFs as catalysts is facilitated through the coordination between metal ions and benzene 1,3,5-tricarboxylic acid (BTC) ligands, resulting in a porous architecture with potential active sites for adsorption and catalysis. Cu^{2+} and Ni^{2+} ions have partially filled d orbitals, which allow them to undergo electronic transitions when they absorb light. In the electromagnetic spectrum, these transitions usually take place in the UV–visible range. The specific wavelengths of light absorbed by Cu^{2+} and Ni^{2+} ions depend on factors such as the ligands surrounding the ion in a complex and the geometry of the complex. The absorption of light by 1,3,5 benzene tricarboxylic acid depends on its molecular structure, which includes conjugated π -electron systems formed by the benzene rings and the carboxylic acid groups. These conjugated systems can absorb light in the UV–visible range due to electronic transitions within the molecule. The specific wavelengths of light absorbed by benzene 1,3,5

tricarboxylic acid will depend on factors such as the existence of functional groups and the electronic environment around the conjugated system. Upon exposure to light, the electrons within these catalysts are elevated to the conduction band from the valence band, creating pairs of electrons and holes ($\bar{e}$ and h^+). Following this, the holes in MOF used as catalysts stay in the valence band and combine with water to create $^{\bullet}OH$ radicals, while the electrons move to the conduction band. Malachite green molecules get attacked by $^{\bullet}OH$ adsorbed onto the surface of the catalyst through interactions with metal sites and organic linkers. Superoxide radicals ($O_2^{\bullet-}$) are created when electrons ($\bar{e}$) in the catalyst's conduction band interact with molecules of oxygen which then react with the adsorbed malachite green. Superoxide radicals ($O_2^{\bullet-}$) and holes (h^+) generated during the photocatalytic process participate in redox reactions with malachite green, causing the dye to break down into smaller, less harmful compounds.(see Fig. 8)

$$M + BTC \rightarrow M(BTC) \quad (M = Ni^{2+} \text{ and } Cu^{2+}) \tag{1}$$

$$M(BTC) + h\upsilon \rightarrow M^{2+} + BTC + e^- + h^+ \tag{2}$$

$$h^+ + H_2O \rightarrow {}^{\cdot}OH + h^+ \tag{3}$$

$${}^{\cdot}OH + Dye \rightarrow \text{Degradation product} \tag{4}$$

$$e^- + O_2 \rightarrow O_2^{\bullet-} \tag{5}$$

$$\text{Adsorbed malachite green} + O_2^{\cdot-} \rightarrow \text{Degradation products} \tag{6}$$

3.7. Antiproliferative evaluation of Cis@Cu-MOF and Cis@Ni-MOF on MDA-MB-231 by MTT assay method

The cytotoxicity of cisplatin encapsulated Cu and Ni-based MOF is assessed by measuring the viability of cells using an MTT (3-(4,5,-dimethylthiazol-2-yl)-2,5-diphenyltetrazolium bromide) assay, that evaluates the mitochondrial function of the cells. The cultured 96-well plate containing both viable and non-viable cells of selected cancerous MDA-MB-23 are kept aside individually for 24 h of inhibition. The selected cell lines are the performed for antiproliferation effect on MDA-MB-231 cell line with the incremental two-fold dilution of various concentrations of Cis@Cu-MOF and Cis@Ni-MOF. The reconstituted MTT solution in PBS is added to Cis@Cu-MOF and Cis@Ni-MOF on the 96 well tissue culture cell plate and untreated control well plates, incubated for several hours and humidified at 37 °C at 5 % CO_2.(see Fig. 9)

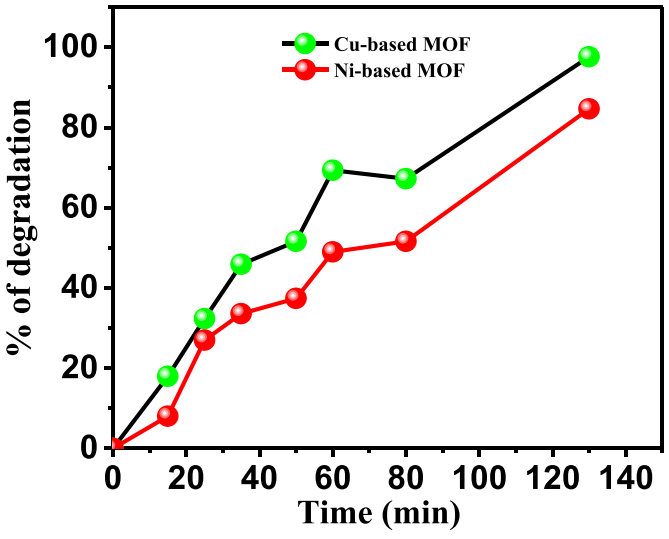

Fig. 8. Time vs % of degradation using Cu and Ni-MOFs.

The tetrazolium ring in MTT is cleaved in active mitochondria, a reaction that only happens in living cells and produces the formazan product. The purple formazan crystal is insoluble in water, hence DMSO is used as a solubilizing solvent for the formazan crystals. The supernatant liquid is ejected out and the dissolved formazan crystals are measured spectrophotometrically at 570 nm. The formazan solution determines the total count and the proportion of living cells is calculated from the triplicate responses done at various concentrations.(see Fig. 10)

$$\textit{Percentage of cellular viability} = \frac{\textit{Average absorbance of treated}}{\text{Average absorbance of control}} \times 100$$

3.7.1. Antiproliferative evaluation of Cis@Cu-MOF against MDA-MB-231

The cisplatin-encapsulated Cu-based MOF is examined on the breast cancer MDA-MB-231 cell line. After 24 h incubation of cultured MBA-MB-231 cell walls, the test samples with different concentrations of 6.25, 12.5, 25, 50 and 100 μg/ml are prepared and tested against the cultured cell walls. The untreated cell walls are taken as control. The MTT dye when added to the cultured 96-well plates of MDA-MB-231 with Cis@Cu-MOF shows a colour change to purple because of the cleavage of tetrazolium rings of MTT dye resulting in insoluble formazan crystals. Initially, when 6.25 μg/ml of Cis@Cu-based MOF is tested, the mitochondrial function of the MDA-MB-231 cell line, the percentage of viability is low at 94.32 %. But when the concentration is increased to 12.5 μg/ml, the percentage of viability is decreased to 79.70 %. With further increase in concentrations to 25, 50 and 100 μg/ml, the viability percentage decreased to 58.72 %, 46.82 % and 34.64 %. As the concentration of Cis@Cu-based MOF, degradation time and incubation period increased, the cellular viability dropped as well. Even at comparatively elevated concentrations (up to 100 μg ml^{-1}), there is still a good viability rate. At greater doses and longer incubation times, it rapidly reduced. Siamak et al. reported Cu-based MOF loaded with Ibuprofen and examined against Caco-2 cells. Caco-2 cells exposed to Cu-MOF/IBU@GM exhibited no toxicity to cells and their survivability remained over 60 % at a concentration of 32 μg/ml. In contrast to Cu-MOF/IBU@GM, at a concentration of 32 μg/ml, Cu-MOF and IBU/Cu-MOF showed substantial damage to Caco-2 cells with a cell viability of around 60 % [45]. But the cisplatin-loaded Cu-based MOF showed a viability of 34.64 against MDA-MB-231 which proved that the Cu-based MOFs are more biocompatible Ibuprofen-loaded Cu-based MOF and it has the potential to serve as a carrier for anticancer drugs.

3.7.2. Antiproliferative evaluation of Cis@Ni-MOF against MDA-MB-231

The evaluation of the cisplatin-encapsulated Ni-based MOF is examined against the MDA-MB-231 cell line. Following a 24-h incubation of the cultured MDA-MB-231 cell wall, test samples with varying concentrations (6.25, 12.5, 25, 50 and 100 μg/ml) are prepared and tested against the cultured cell walls. The untreated cell walls served as the control. The MTT dye when added to the cultured 96-well plates of MDA-MB-231 with Cis@Cu-MOF and Cis@Ni-MOF shows a colour change to purple because of the cleavage of tetrazolium rings of MTT dye resulting in insoluble formazan crystals. Initially, when testing 6.25 μg/ml of Cis@Ni-based MOF, the mitochondrial function of the MDA-MB-231 cell line showed a high viability percentage of 94.47 %. However, as the concentration increased to 12.5 μg/ml, the viability percentage lowered to 82.47 %. Subsequent concentration increases to 25, 50 and 100 μg/ml resulted in survival percentages of 59.56 %, 50.01 % and 37.87 %, respectively. The cellular viability decreased with higher concentrations of Cis@Ni-based MOF, longer degradation times and extended incubation periods. Even at elevated concentrations (up to

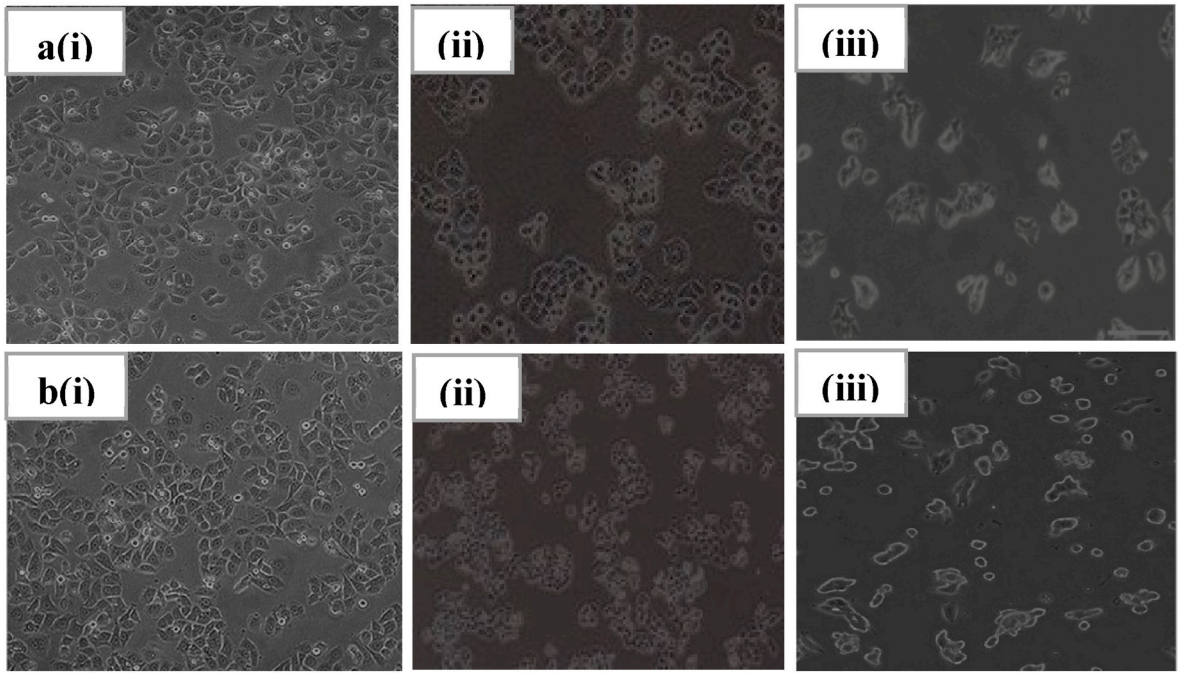

Fig. 9. MDA-MB-231 cell line treated with various concentrations of a (i-iii) Cis@Cu-MOF b (i-iii) Cis@Ni-MOF

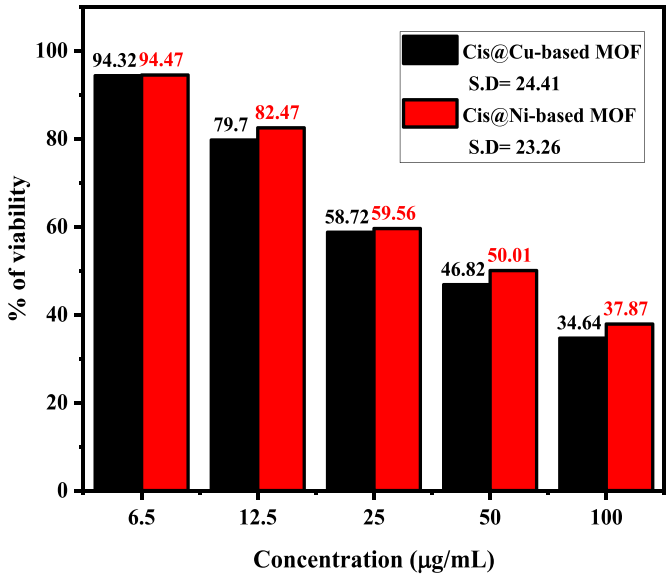

Fig. 10. Graphical representation of Cis@Cu-based and Cis@Ni-based MOFs.

100 µg ml^{-1}), a relatively good viability rate is maintained, but it decreases rapidly at greater doses and longer incubation times.

However, at a higher concentration of 100 µg/ml, the percentage of inhibition of Cis@Cu-based MOF is greater compared to Cis@Ni-based MOF. Compared to Cis@Ni-based MOF, the Cis@Cu-based MOF acted as a good drug carrier, because the loading of cisplatin drug in Cu-based MOF is 23.47 % which is higher than Ni-based MOF of 18.24 % which delivers a larger amount of cisplatin and caused damage only to the DNA of cancer cells and prevents its cell replication and it did not affect normal cell line when tested against L-929. Based on the MTT assay, it is concluded that Cu and Ni-based MOFs loaded with cisplatin affected the mitochondrial cell function of MDA-MB-231 and potentially improved therapeutic effects without causing damage to the mitochondrial cell function of the normal cell line tested against L-929. Additionally, an increase in concentration led to a rise in the percentage of growth inhibition, ranging from 5.53 % to 62.13 % using Cis@Ni-based MOF and 5.68 %–65.36 % using Cis@Cu-based MOF. The IC_{50} value of Cis@Cu-based MOF is 47.77 µg/ml and for Cis@Ni-based MOF is 55.31 µg/ml. Moosareza et al. produced a metal-organic framework based on lanthanum, employing 3,4-hydroxycinnamic acid as a ligand. The La-based MOF demonstrated good biocompatibility with the cell line of human breast cancer, MDA-MB-468. Remarkably, following treatment with 3,4-DHCA employing La-based MOF, 40.35 % of the MDA-MB-468 cells are still alive. The findings imply that La-based MOF is a feasible method for anticancer drug delivery [46]. Similar results were also reported by Hatin et al., using benzene 1,4 dicarboxylic acid as a ligand loaded with anticancer drug Cisplatin [47]. However, the Ni-based MOF loaded with cisplatin demonstrated a 37.87 % viability against MDA-MB-231, demonstrating that Ni-based MOFs are more biocompatible than La-based MOFs and have the potential to be used as anticancer drug carriers. The standard deviation of Cis@Cu-MOF and Cis@Ni-MOF was 24.41 and 23.26.

3.7.3. Drug release study

Controlled drug release is crucial for drug administration. In vitro Cisplatin release kinetics of the Cisplatin loaded Cu and Ni-based MOFs were preliminarily investigated in PBS of pH 7.4 at 37 °C. As expected, Cu and Ni-based MOFs loaded with 23.47 % and 18.24 % of Cisplatin showed controlled drug release behavior in PBS solution. As it can be seen from the drug release kinetics Fig. 11, the complete release of Cisplatin from Cu and Ni-based MOFs was achieved after 72 h. This value is similar to the reported MIL-100(Cr) for IBU release [48]. According to the profile, about 29.7 % and 24.2 % of Cisplatin was released after 3 h from Cu and Ni-based MOFs. Finally, after 72 h about 94.4 % and 89.7 % of Cisplatin was released from Cu and Ni-based MOFs. These results demonstrated that the as-synthesized Cu and Ni-based MOFs are excellent candidates for targeted drug delivery.(See Table 3)

4. Conclusion

The study describes the synthesis and various analyses of Cu and Ni-based Metal-Organic Frameworks (MOFs) using a hydrothermal method

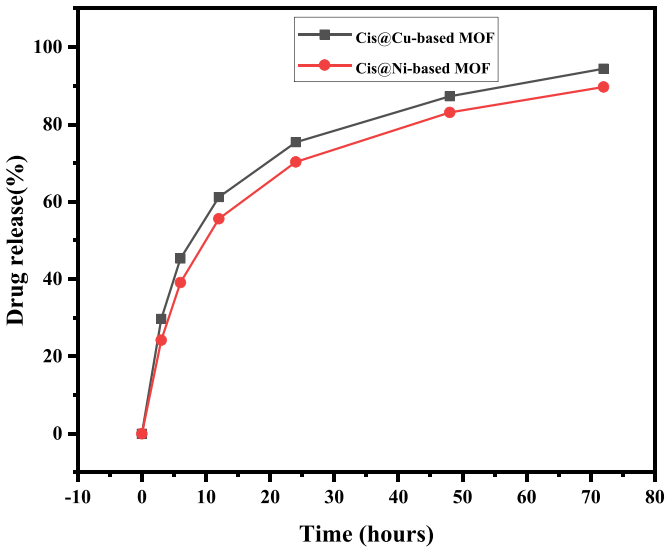

Fig. 11. Cisplatin release process from Cu and Ni-based MOFs in PBS of pH 7.4.

in a stainless-steel Teflon autoclave. The outcome demonstrated that Cu-based MOFs exhibited a higher degradation percentage of 97.61 % after 130 min compared to Ni-based MOFs, which only achieved 84.76 % degradation in the same time frame, this indicates the greater efficiency of Cu-based MOFs for pollutant degradation. Additionally, the study investigated the antiproliferative effect of Cisplatin-loaded Cu and Ni-based MOFs against the breast cancer MDA-MB-231 cell line by MTT assay. At a higher concentration of 100 μg/ml, Cis@Cu-based MOFs showed a cell viability of 34.64 % and Cis@Ni-based MOFs showed 37.87 % viability. The IC_{50} values for Cis@Cu-based and Cis@Ni-based MOFs are determined to be 47.77 μg/ml and 55.31 μg/ml, respectively. These findings suggest that both Cu and Ni-based MOFs have potential as drug delivery systems for cancer treatment, with Cu-based MOFs exhibiting slightly higher efficacy. Overall, the findings lay the groundwork for further research aimed at harnessing the unique properties of MOFs for addressing environmental challenges and advancing biomedical treatments.

CRediT authorship contribution statement

A.H. Hatin Betseba: Writing – original draft, Validation, Methodology, Formal analysis, Data curation, Conceptualization. **Y. Christabel Shaji:** Writing – review & editing, Visualization, Validation, Supervision, Software, Resources, Project administration, Methodology, Investigation, Funding acquisition, Conceptualization.

Declaration of competing interest

The authors declare that they have no known competing financial interests or personal relationships that could have appeared to influence the work reported in this paper.

Acknowledgment

The corresponding author Y. Christabel Shaji likes to thank Crossian Research Forum **(Seed Money Scheme No-CRF/2022-10)**, Holy Cross College (Autonomous), Nagercoil, Tamilnadu 629004, India, for providing research grant for the execution of this research work.

Data availability

Data will be made available on request.

References

[1] F.J. Heiligtag, M. Niederberger, The fascinating world of nanoparticle research, Mater. Today 16 (2013) 262–271, https://doi.org/10.1016/j.mattod.2013.07.004.g.
[2] H. Furukawa, K.E. Cordova, M.O. Keeffe, O.M. Yaghi, The chemistry and applications of Metal-organic framework, Sci. Technol. Humanit. 341 (2013) 1230444, https://doi.org/10.1126/science.1230444.
[3] R. Zhao, Z. Liang, R. Zou, Q. Xu, Metal-organic frameworks for batteries, Joule 2 (2018) 1–25, https://doi.org/10.1016/j.joule.2018.09.019.
[4] Y. Xu, Q. Li, X. Guo, S. Zhang, W. Li, H. Pang, Metal-organic frameworks and their composites for supercapacitor application, J. Energy Storage 56 (2022) 105819, https://doi.org/10.1016/j.est.2022.105819.
[5] T. Jia, Y. Gu, F. Li, Progress and potential of metal-organic frameworks (MOFs) for gas storage and separation: a review, J. Environ. Chem. Eng. 10 (2022) 108300, https://doi.org/10.1016/j.jece.2022.108300.
[6] A. Wang, M. Walden, R. Ettlinger, F. Kiessling, J. Gassensmith, T. Lammers, S. Wuttke, Q. Pena, Biomedical metal-organic framework materials: perspectives and challenges, Adv. Funct. Mater. 2308589. https://doi.org/10.1002/adfm.202308589.
[7] W. Koo, J. Jang, I. Kim, Metal-organic frameworks for chemiresistive sensors, Chem 5 (2019) 1938–1963, https://doi.org/10.1016/j.chempr.2019.04.013.
[8] A. Li, Q. Gao, J. Xu, X. Bu, Proton-conductive metal-organic frameworks: recent advances and perspectives, Coord. Chem. Rev. 344 (2017) 54–82, https://doi.org/10.1016/j.ccr.2017.03.027.
[9] D. Li, H. Xu, L. Jiao, H. Jiang, Metal-organic frameworks for catalysis: state of the art, challenges, and opportunities, EnergyChem 1 (2019) 100005, https://doi.org/10.1016/j.enchem.2019.100005.
[10] S. Saglam, F.N. Turk, H. Arslanoglu, Use and applications of metal-organic frameworks (MOF) in dye adsorption: review, J. Environ. Chem. Eng. 11 (2023) 110568, https://doi.org/10.1016/j.jece.2023.110568.
[11] K. Liu, F. Bigdeli, Z. Sharifzadeh, S. Gholizadeh, A. Morsali, Role of metal-organic framework composites in removal of inorganic toxic contaminants, J. Clean. Prod. 404 (2023) 136709, https://doi.org/10.1016/j.jclepro.2023.136709.
[12] A. Azanaw, B. Birlie, B. Teshome, M. Jemberie, Textile effluent treatment methods and eco-friendly resolution of textile wastewater, Case Stud. Chem. Environ. Eng. 6 (2022) 100230, https://doi.org/10.1016/j.cscee.2022.100230.
[13] R. Al-Tohamy, S.S. Ali, F. Li, K.M. Okasha, Y.A.G. Mahmoud, T. Elsamahy, H. Jiao, Y. Fu, J. Sun, A critical review on the treatment of dye-containing wastewater: ecotoxicological and health concerns of textile dyes and possible remediation approaches for environmental safety, Ecotoxicol. Environ. Saf. 231 (2022) 113160, https://doi.org/10.1016/j.ecoenv.2021.113160.
[14] S.J. Culp, F.A. Beland, Malachite green: a toxicological review, J. Am. Coll. Toxicol. 15 (199) 219-238. https://doi.org/10.3109/10915819609008715.
[15] S. Srivastava, R. Sinha, D. Roy, Toxicological effects of malachite green, Aquat. Toxicol. 66 (2004) 319–329, https://doi.org/10.1016/j.aquatox.2003.09.008.
[16] N.S. Abdul Mubarak, K.Y. Foo, R. Schneider, R.M. Abdelhameed, S. Sabar, The chemistry of MIL-125 based materials: structure, synthesis, modification strategies and photocatalytic applications, J. Environ. Chem. Eng. 10 (2022) 106883, https://doi.org/10.1016/j.jece.2021.106883.
[17] B. Bouider, S. Haffad, B.S. Bouakaz, M. Berd, S. Ouhnia, A. Habi, MOF-5/Graphene oxide composite photocatalyst for enhanced photocatalytic activity of methylene blue degradation under solar light, J. Inorg. Organomet. Polym. 33 (2023) 4001–4011, https://doi.org/10.1007/s10904-023-02668-y.
[18] X. Li, Y. Wang, Q. Guo, Porous NH_2-MIL-101(Fe) metal-organic framework for effective photocatalytic degradation of azo dye in wastewater treatment, Heliyon 8 (2022) e09942, https://doi.org/10.1016/j.heliyon.2022.e09942.
[19] X. Tong, S. Wang, J. Zuo, Y. Ge, Q. Gao, S. Liu, J. Ding, F. Liu, J. Luo, J. Xiong, Two 2D uranyl coordination complexes showing effective photocatalytic degradation of rhodamine B and mechanism study, Chin. Chem. Lett. 32 (2021) 604–608, https://doi.org/10.1016/j.cclet.2020.11.044.
[20] A. Rafiq, M. Ikram, S. Ali, F. Niaz, M. Khan, Q. Khan, M. Maqbool, Photocatalytic degradation of dyes using semiconductor photocatalysts to clean industrial water pollution, J. Ind. Eng. Chem. 97 (2021) 111–128, https://doi.org/10.1016/j.jiec.2021.02.017.
[21] H. Zhao, Q. Xia, H. Xing, D. Chen, H. Wang, Construction of pillared-layer MOF as efficient visible-light photocatalysts for aqueous Cr(VI) reduction and dye degradation, ACS Sustainable Chem. Eng. 5 (2017) 4449–4456, https://doi.org/10.1021/acssuschemeng.7b00641.
[22] F. Bray, J. Ferlay, I. Soerjomataram, R.L. Siegel, L.A. Torre, A. Jemal, Global cancer statistics 2018: GLOBOCAN estimates of incidence and mortality worldwide for 36 cancers in 185 countries, CA Cancer J. Clin. 68 (2018) 394–424, https://doi.org/10.3322/caac.2149226.
[23] X. Dai, L. Xiang, T. Li, Z. Bai, Cancer hallmarks, biomarkers and breast cancer molecular subtypes, J. Cancer 7 (2016) 1281–1294, https://doi.org/10.7150/jca.13141.
[24] J. He, T. Peng, Y. Peng, L. Ai, Z. Deng, X.Q. Wang, W. Tan, Mocularly engineering triptolide with aptamers for high specificity and cytotoxicity for triple-negative breast cancer, J. Am. Chem. Soc. 142 (2020) 2699–2703, https://doi.org/10.1021/jacs.9b10510.
[25] J. Hao, I.S. Stavljenic Milasin, Z.B. Eken, M. Marinka-Stipetic, K. Pavelic, F. Ozer, Effects of zeolite as a drug delivery system on cancer therapy: a systematic review, Molecules (Basel) 26 (2021) 6196, https://doi.org/10.3390/molecules26206196.
[26] K.S. Park, Z. Ni, A.P. Cote, J.Y. Choi, R. Huang, F.J. Uribe-Romo, H.K. Chae, M. O. Keeffe, O.M. Yaghi, Exceptional chemical and thermal stability of zeolitic

imidazolate frameworks, Proc. Natl. Acad. Sci. USA 103 (2006) 10186–10191, https://doi.org/10.1073/pnas.0602439103.
[27] Q. Wang, Y. Sun, S. Li, P. Zhang, Q. Yao, Synthesis and modification of ZIF-8 and its application in drug delivery and tumor therapy, RSC Adv. 10 (2020) 37600–37620, https://doi.org/10.1039/d0ra07950b.
[28] C.Y. Sun, C. Qin, X.L. Wang, G.S. Yang, K.Z. Shao, Y.Q. Lan, Z.M. Su, P. Huang, C. G. Wang, E.B. Wang, Zeolitic imidazolate framework-8 as efficient pH-sensitive drug delivery vehicle, Dalton Trans. 41 (2012) 6906–6909, https://doi.org/10.1039/C2DT30357D.
[29] M.S. Samuel, K.V. Savunthari, S. Ethiraj, Synthesis of a copper (II) metal-organic framework for photocatalytic degradation of rhodamine B dye in water, Environ. Sci. Pollut. Res. Int. 28 (2021) 40835–40843, https://doi.org/10.1007/s11356-021-13571-9.
[30] M.G. Radhika, B. Gopalakrishna, K. Chaitra, L.K.G. Bhatta, K. Venkatesh, M. K. Sudha Kamath, N. Kathyayini, Electrochemical studies on Ni, Co & Ni/Co-MOFs for high-performance hybrid supercapacitors, Mater. Res. Express 7 (2020) 054003, https://doi.org/10.1088/2053-1591/ab8d5d.
[31] C.X. Liu, W.H. Zhang, N. Wang, P. Guo, M. Muhler, Y. Wang, S. Lin, Z. Chen, G. Yang, Highly efficient photocatalytic degradation of dyes by a copper-triazolate metal-organic framework, Chemistry 13 (24) (2018) 16804–16813, https://doi.org/10.1002/chem.201803306.
[32] C.I. Ezugwu, M.A. Asraf, X. Li, S. Liu, C. Kao, S. Zhuiykov, F. Verpoort, Cationic nickel metal-organic frameworks for adsorption of negatively charged dye molecules, F, Data Brief 18 (2018) 1952–1961, https://doi.org/10.1016/j.dib.2018.04.062.
[33] A.S. Eliwa, A.E. Ali, W.M. Hosny, G.G. Mohamed, R.G. Deghadi, Sonochemical synthesis and characterization of novel copper-based metal-organic framework: its application as an electrochemical sensor for determination of Cd(II) ion in real water samples, Inorg. Chem. Commun. 153 (2023) 110733, https://doi.org/10.1016/j.inoche.2023.110733.
[34] P. Du, Y. Dong, C. Liu, W. Wei, D. Liu, P. Liu, Fabrication of hierarchical porous nickel-based metal-organic framework (Ni-MOF) constructed with nanosheets as novel pseudo-capacitive material for asymmetric supercapacitor, J. Colloid Interface Sci. 518 (2018) 57–68, https://doi.org/10.1016/j.jcis.2018.02.010.
[35] A. Kojtari, H.F. Ji, Metal-organic framework micro/nanopillars of Cu(BTC).3H_2O and Zn(ADC).DMSO, Nanomaterials (Basel) 5 (2015) 565–567, https://doi.org/10.3390/nano5020565.
[36] K. Ma, C. Bi, X. Zhang, Z. Zong, C. Fan, C. Xu, Y.H. Fan, Synthesis of two different Ni(II) coordination polymers by introduction of carboxylic acid ligands: crystal structure and photocatalytic properties, Inorg. Chim. Acta. 494 (2019) 91–97, https://doi.org/10.1016/j.ica.2019.04.042.
[37] J. Zhong, J. Zhou, M. Xiao, J. Liu, J. Shen, J. Liu, S. Ren, Design and syntheses of functionalized copper-based MOFs and its adsorption behavior for Pb(II), Chin. Chem. Lett. 33 (2022) 973–978, https://doi.org/10.1016/j.cclet.2021.07.040.
[38] F. Israr, D. Chun, Y. Kim, D.K. Kim, High yield synthesis of Ni-BTC metal-organic framework with ultrasonic irradiation: role of polar aprotic DMF solvent, Ultrason. Sonochem. 31 (2016) 93–101, https://doi.org/10.1016/j.ultsonch.2015.12.007.
[39] N. Nayak, S. Singha, J.P. Maity, P.P. Rath, T. Sahoo, T.R. Sahoo, Photocatalytic degradation of malachite green dye under solar light irradiation using ZnO and ZnO-TiO_2 nanoparticles, J. Mater. Sci. Mater. Electron. 35 (2024) 310, https://doi.org/10.1007/s10854-024-12066-w.
[40] D. Yao, X. Xie, X. Liang, S. Lu, H. Lai, Photocatalytic degradation of malachite green by titanium dioxide/covalent organic framework composite: characterization, performance and mechanism, ChemistryOpen (2024), https://doi.org/10.1002/open.202300209.
[41] J.J. Du, Y.P. Yuan, J.X. Sun, F.M. Peng, X. Jiang, L.G. Qiu, A.J. Xie, Y.H. Shen, J. F. Zhu, New photocatalysts based on MIL-53 metal-organic frameworks for the decolorization of methylene blue dye, J. Hazard. Mater. 190 (2011) 945–951, https://doi.org/10.1016/j.jhazmat.2011.04.029.
[42] N.M. Mahmoodi, J. Abdi, Nanoporous metal-organic framework (MOF-199): Synthesis, characterization and photocatalytic degradation of basic blue 41, Microchem. J. 144 (2018) 436–442, https://doi.org/10.1016/j.microc.2018.09.033.
[43] C.F. Zhang, L.G. Qiu, F. Ke, Y.J. Zhu, Y.P. Yuan, G.S. Xu, X. Jiang, A novel magnetic recyclable photocatalyst based on a core-hell metal-organic framework Fe_3O_4@ MIL-100 (Fe) for the decolorization of methylene blue dye, J. Mater. Chem. A 1 (2013) 14329–14334, https://doi.org/10.1039/C3TA13030D.
[44] J. Gascon, M.D. Hernandez-Alonso, A.R. Almeida, G.P.M. van Klink, F. Kapteijn, G. Mul, Isoreticular MOFs as efficient photocatalysts with tunable band gap: an operando FTIR study of the photoinduced oxidation of propylene, ChemSusChem 1 (2008) 981–983, https://doi.org/10.1002/cssc.200800203.
[45] S. Javanbakht, M. Pooresmaeil, H. Hashemi, H. Namazi, Carboxymethylcellulose capsulated Cu-based metal-organic framework-drug nanohybrid as a pH-sensitive nanocomposite for ibuprofen oral delivery, Int. J. Biol. Macromol. 119 (2018) 588–596, https://doi.org/10.1016/j.ijbiomac.2018.07.181.
[46] M. Safinejad, A. Rigi, M. Zeraati, Z. Heidary, S. Jahani, N.P.S. Chauhan, G. Sargazi, Lanthanum-based metal-organic framework (La-MOF) use of 3,4-dihydroxycinnamic acid as drug delivery system linkers in human breast cancer therapy, BMC Chem. 16 (2022) 93, https://doi.org/10.1186/s13065-022-00886-y.
[47] A. Hatin Betseba, Y. Christabel Shaji, Y. Brucely, K. Sakthipandi, Synthesis and characterization of nickel-based MOFs: enhancing photocatalysis and targeted cancer drug delivery, J. Indian Chem. Soc. 101 (10) (2024) 101335, https://doi.org/10.1016/j.jics.2024.101335.
[48] P. Horcajada, C. Serre, M. Vallet-Regi, M. Sebban, F. Taulelle, G. Ferey, Metal-organic frameworks as efficient materials for drug delivery, Angew. Chem., Int. Ed. 45 (2006) 5974–5978, https://doi.org/10.1002/anie.200601878.